RSC Advances

PAPER

View Article Online
View Journal | View Issue

Open Access Article. Published on 28 August 2020. Downloaded on 5/25/2026 2:33:50 PM.
This article is licensed under a Creative Commons Attribution-NonCommercial 3.0 Unported Licence.

Check for updates

Cite this: *RSC Adv.*, 2020, **10**, 32069

Heterodinuclear nickel(II)–iron(II) azadithiolates as structural and functional models for the active site of [NiFe]-hydrogenases†

Li-Cheng Song, *[ab] Bei-Bei Liu,[a] Wen-Bo Liu[a] and Zheng-Lei Tan[a]

Received 15th May 2020
Accepted 20th August 2020

DOI: 10.1039/d0ra04344c

rsc.li/rsc-advances

To develop the biomimetic chemistry of [NiFe]-H_2ases, the first azadithiolato-bridged NiFe model complexes $[CpNi\{(\mu\text{-}SCH_2)_2NR\}Fe(CO)(diphos)]BF_4$ (**5**, R = Ph, diphos = dppv; **6**, 4-ClC_6H_4, dppv; **7**, 4-MeC_6H_4, dppv; **8**, CO_2CH_2Ph, dppe; **9**, H, dppe) have been synthesized *via* well-designed synthetic routes. Thus, treatment of $RN[CH_2S(O)CMe]_2$ with *t*-BuONa followed by reaction of the resulting intermediates $RN(CH_2SNa)_2$ with $(dppv)Fe(CO)_2Cl_2$ or $(dppe)Fe(CO)_2Cl_2$ gave the N-substituted azadithiolato-chelated Fe complexes $[RN(CH_2S)_2]Fe(CO)_2(diphos)$ (**1**, R = Ph, diphos = dppv; **2**, 4-ClC_6H_4, dppv; **3**, 4-MeC_6H_4, dppv; **4**, CO_2CH_2Ph, dppe). Further treatment of **1–4** with nickelocene in the presence of $HBF_4\cdot Et_2O$ afforded the corresponding N-substituted azadithiolato-bridged NiFe model complexes **5–8**, while treatment of **8** with $HBF_4\cdot Et_2O$ resulted in formation of the parent azadithiolato-bridged model complex **9**. While all the new complexes **1–9** were characterized by elemental analysis and spectroscopy, the molecular structures of model complexes **6–8** were confirmed by X-ray crystallographic study. In addition, model complexes **7** and **9** were found to be catalysts for H_2 production with moderate i_{cat}/i_p and overpotential values from TFA under CV conditions.

Introduction

[NiFe]-hydrogenases ([NiFe]-H_2ases) are a class of biological enzymes that catalyze the reversible redox reaction between molecular H_2 and protons in a variety of microorganisms such as bacteria, archaea, and cyanobacteria.[1–3] An X-ray crystallographic study revealed that the active site of [NiFe]-H_2ases features a Ni(tetracysteinate) moiety, in which the two cysteinate atoms are connected to the Fe atom of an $Fe(CN)_2(CO)$ moiety. In addition, the oxidized state of [NiFe]-H_2ases includes an additional bridging oxygenous ligand, while the reduced state of [NiFe]-H_2ases contains an additional bridging hydride ligand or a Ni–Fe metal–metal bond (Fig. 1).[4–6]

In recent years, molecular H_2 has been considered as an ideal energy source to replace fossil fuels to solve the current energy shortage and environmental pollution problems. This is because dihydrogen is a high energy-dense, clean-burning, and sustainable energy.[7–9] In addition, although H_2 production can be carried out in an industry scale from fossil fuel by petroleum reforming, the utilized catalyst is the expensive and relatively scarce noble metal Pt. To develop the biomimetic chemistry of [NiFe]-H_2ases and to search for the water splitting H_2-producing catalysts that contain the earth-abundant and cheap metals such as iron and nickel present in the active site of [NiFe]-H_2ases, synthetic chemists have prepared a wide variety of biomimetic models for [NiFe]-H_2ases.[9–29] However, among the prepared models no one bears a bridging azadithiolato ligand between their NiFe centers. In view of the important catalytic role played by the central N atom of the bridging azadithiolato ligand in the active site of [FeFe]-H_2ases,[30–32] we recently launched a study on the preparation of the first azadithiolato ligand-containing [NiFe]-H_2ase models. Fortunately, we have successfully prepared and characterized such a type of azadithiolato-bridged models in which each contains an azadithiolato $RN(CH_2S)_2$ ligand bridged between their CpNi and (diphos)(CO)Fe units (Fig. 2). In addition, the two representative

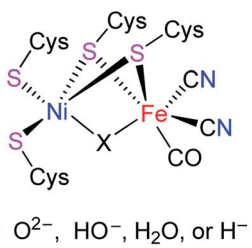

Fig. 1 Active site of [NiFe]-H_2ases.

[a]Department of Chemistry, State Key Laboratory of Elemento-Organic Chemistry, College of Chemistry, Nankai University, Tianjin 300071, China. E-mail: lcsong@nankai.edu.cn

[b]Collaborative Innovation Center of Chemical Science and Engineering (Tianjin), Tianjin 300072, China

† Electronic supplementary information (ESI) available: Some electrocatalytic plots/data (Fig. S1–S3/Table S1) and some IR/NMR spectra (Fig. S4–S23). CCDC 2001290–2001292. For ESI and crystallographic data in CIF or other electronic format see DOI: 10.1039/d0ra04344c

Open Access Article. Published on 28 August 2020. Downloaded on 5/25/2026 2:33:50 PM.
This article is licensed under a Creative Commons Attribution-NonCommercial 3.0 Unported Licence.

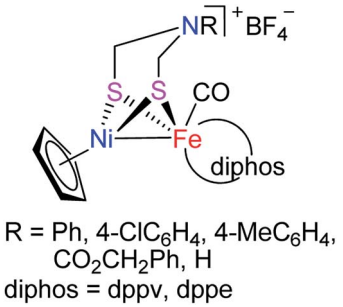

Fig. 2 Models of [NiFe]-H_2ases reported in this article.

models have been found to be catalysts for proton reduction to hydrogen under electrochemical conditions. Herein, we report the interesting results obtained by this study.

Results and discussion

Synthesis and characterization of precursor complexes $[RN(CH_2S)_2]Fe(CO)_2(diphos)$ (1–4)

The N-substituted azadithiolato ligand-chelated mononuclear Fe complexes **1–4** utilized for the preparation of the targeted [NiFe]-H_2ase models could be prepared by one-pot reactions of the bis(thioester) compounds $RN[CH_2S(O)CMe]_2$ (R = Ph, 4-ClC_6H_4, 4-MeC_6H_4, CO_2CH_2Ph) with *tert*-butoxysodium in THF at −78 °C followed by treatment of the resulting disodium mercaptides $RN(CH_2SNa)_2$ with (dppv)$Fe(CO)_2Cl_2$ or (dppe)$Fe(CO)_2Cl_2$ generated *in situ* by reaction of an acetone solution of $FeCl_2$ with the corresponding diphosphine and bubbling CO gas[33,34] in 18–35% yields (Scheme 1).

Precursor complexes **1–4** are air-stable, brown-red solids and have been characterized by elemental analysis and various spectroscopic methods. For example, the ^{1}H NMR spectra of **1–3** each displayed one singlet in the region 4.56–4.63 ppm for the four H atoms in their azadithiolato methylene groups, whereas the ^{1}H NMR spectrum of **4** displayed a multiplet in the range 4.89–5.30 ppm for the four H atoms in its azadithiolato methylene groups. The $^{13}C\{^1H\}$ NMR spectra of **1–4** exhibited one or two singlets in the range 200–214 ppm for their two terminal carbonyl C atoms, whereas the $^{31}P\{^1H\}$ NMR spectra of **1–3** displayed one singlet at about 79 ppm for the two P atoms in their dppv ligands and the $^{31}P\{^1H\}$ NMR spectrum of **4** exhibited one singlet at 44.3 ppm for the two P atoms in its dppe ligand. In addition, the IR spectra of **1–4** showed two absorption bands in the range 2035–1968 cm^{-1} for their two terminal carbonyls.

Synthesis and characterization of targeted [NiFe]-H_2ase models $[CpNi\{(\mu\text{-}SCH_2)_2NR\}Fe(CO)(diphos)]BF_4$ (5–9)

Interestingly, the targeted N-substituted dithiolato-bridged NiFe-based models **5–8** were found to be prepared by treatment of the mononuclear Fe complexes **1–4** with nickelocene/$HBF_4\cdot Et_2O$ in a mixed solvent CH_2Cl_2/Et_2O at room temperature in 21%–62% yields (Scheme 2). Further treatment of the N-substituted dithiolato-bridged model complex **8** with $HBF_4\cdot Et_2O$ in a mixed solvent CH_2Cl_2/PhOMe at room temperature gave rise to the parent azadithiolato-bridged model **9** in 42% yield (Scheme 3). As shown in Schemes 2 and 3, while model **9** can be formally viewed as produced through the selective acidolysis of the N–C(=O) bond rather than O–C(=O) bond of model **8**, model complexes **5–8** might be regarded as produced *via* two elementary reaction steps. The first step involves protonation of one anionic cyclopentadienyl ligand in Cp_2Ni to give cyclopentadiene and cyclopentadienylnickel tetrafluoroborate.[35,36] The second step involves coordination of the two S atoms in complexes **1–4** to Ni atom of the *in situ* formed intermediate $CpNi(BF_4)$ followed by loss of one CO ligand from **1–4** to give the final products.

Model complexes **5–9** are also air-stable, brown-red solids. They were characterized by the IR, ^{1}H NMR, $^{13}C\{^1H\}$ NMR, and

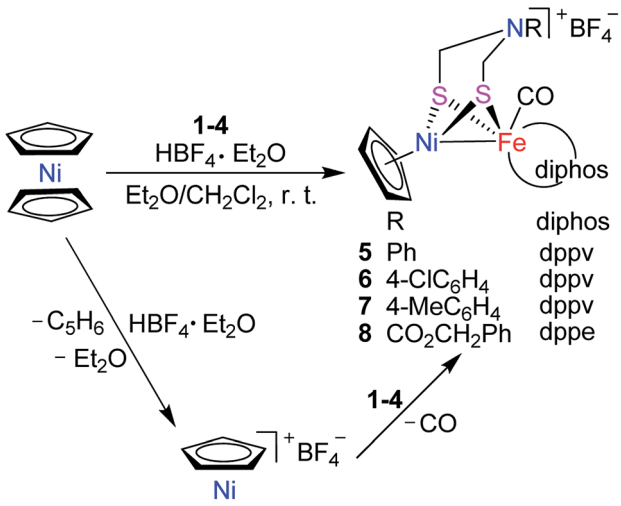

Scheme 2 Synthesis of targeted models **5–8**.

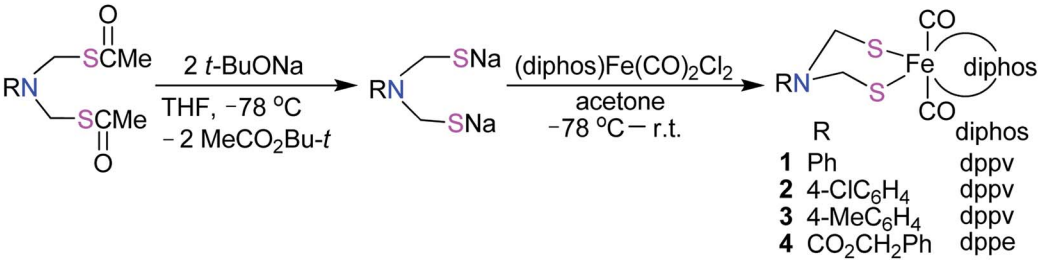

Scheme 1 Synthesis of precursor complexes **1–4**.

Open Access Article. Published on 28 August 2020. Downloaded on 5/25/2026 2:33:50 PM.
This article is licensed under a Creative Commons Attribution-NonCommercial 3.0 Unported Licence.

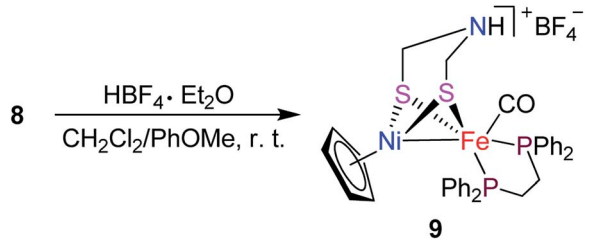

Scheme 3 Synthesis of targeted model **9**.

$^{31}P\{^1H\}$ NMR spectroscopic techniques and elemental analysis. For instance, the IR spectra of **5–9** showed one strong absorption band in the region 1956–1939 cm^{-1} for their terminal carbonyls, which are close to that (1944 cm^{-1}) displayed by the [NiFe]-H_2ase from *D. Vulgaris* Miyazaki F.[37] The ^1H NMR spectra of **5–9** displayed one singlet in the range 4.42–4.61 ppm for the five H atoms in their Cp rings. In addition, the $^{13}C\{^1H\}$ NMR spectra of **5–9** exhibited one singlet in the region 206–220 ppm for their terminal carbonyl C atoms, whereas the $^{31}P\{^1H\}$ NMR spectra of **5–7** displayed one singlet in the region 82.7–83.9 ppm for the two P atoms in their dppv ligands and those of **8** and **9** exhibited the corresponding signals in the range 78.1–79.1 ppm for the two P atoms in their dppe ligands.

The molecular structures of the azadithiolato-bridged complexes **6–8** were confirmed by X-ray crystallographic analysis. While Fig. 3–5 show their molecular structures, Table 1 lists their selected bond lengths and angles. As shown in Fig. 3–5, the three biomimetic models are indeed the azadithiolato ligand-containing complexes that are composed of one monocation $[CpNi\{(\mu\text{-}SCH_2)_2NC_6H_4Cl\text{-}4\}Fe(CO)(dppv)]^+$, $[CpNi\{(\mu\text{-}SCH_2)_2NC_6H_4Me\text{-}4\}Fe(CO)(dppv)]^+$, or $[CpNi\{(\mu\text{-}SCH_2)_2\text{-}NCO_2CH_2Ph\}Fe(CO)(dppe)]^+$ and one monoanion BF_4^-. Since the molecular structures of **6** and **7** are virtually the same as that of **8** (except that the 4-ClC_6H_4/dppv in **6** and 4-MeC_6H_4/dppv in **7** are replaced by the CO_2CH_2Ph/dppe in **8**), we just discuss the structure of **8**. In the monocation of **8**, the Ni–Fe distance (2.5036 Å) is shorter than that (2.57 Å) of the [NiFe]-H_2ase from *D. Vulgaris* Miyazaki F[38] and the sum (2.56 Å) of the Ni and Fe covalent radii,[39] indicative of the presence of a Ni–Fe metal–metal bond. In addition, the Ni–Fe distance of **8** is very close to

Table 1 Selected bond lengths (Å) and angles (°) for **6–8**

6			
Ni(1)–Fe(1)	2.5033(9)	Fe(1)–S(1)	2.2472(12)
Ni(1)–S(1)	2.1783(13)	Fe(1)–S(2)	2.2361(11)
Ni(1)–S(2)	2.1770(11)	Fe(1)–P(1)	2.2198(11)
N(1)–C(28)	1.433(5)	Fe(1)–P(2)	2.2215(12)
Ni(1)–S(1)–Fe(1)	68.87(4)	S(2)–Fe(1)–S(1)	87.09(4)
Ni(1)–S(2)–Fe(1)	69.10(4)	S(2)–Fe(1)–Ni(1)	54.34(3)
S(2)–Ni(1)–S(1)	90.34(4)	S(1)–Fe(1)–Ni(1)	54.26(3)
P(1)–Fe(1)–P(2)	86.10(4)	S(1)–Ni(1)–Fe(1)	56.86(4)
7			
Ni(1)–Fe(1)	2.5071(9)	Fe(1)–S(1)	2.2497(14)
Ni(1)–S(1)	2.1826(16)	Fe(1)–S(2)	2.2374(13)
Ni(1)–S(2)	2.1795(14)	Fe(1)–P(1)	2.2268(15)
N(1)–C(33)	1.429(7)	Fe(1)–P(2)	2.2249(14)
Ni(1)–S(1)–Fe(1)	68.88(5)	S(2)–Fe(1)–S(1)	87.15(5)
Ni(1)–S(2)–Fe(1)	69.15(4)	S(2)–Fe(1)–Ni(1)	54.33(4)
S(2)–Ni(1)–S(1)	90.31(5)	S(1)–Fe(1)–Ni(1)	54.30(4)
P(1)–Fe(1)–P(2)	86.13(5)	S(1)–Ni(1)–Fe(1)	56.83(4)
8			
Ni(1)–Fe(1)	2.5036(9)	Fe(1)–S(1)	2.2367(11)
Ni(1)–S(1)	2.1807(13)	Fe(1)–S(2)	2.2306(12)
Ni(1)–S(2)	2.1819(12)	Fe(1)–P(1)	2.2433(12)
N(1)–C(34)	1.434(5)	Fe(1)–P(2)	2.2242(11)
Ni(1)–S(1)–Fe(1)	69.04(4)	S(2)–Fe(1)–S(1)	87.28(4)
Ni(1)–S(2)–Fe(1)	69.13(4)	S(2)–Fe(1)–Ni(1)	54.52(4)
S(1)–Ni(1)–S(2)	89.93(4)	S(1)–Fe(1)–Ni(1)	54.43(3)
P(1)–Fe(1)–P(2)	87.08(4)	S(1)–Ni(1)–Fe(1)	56.54(4)

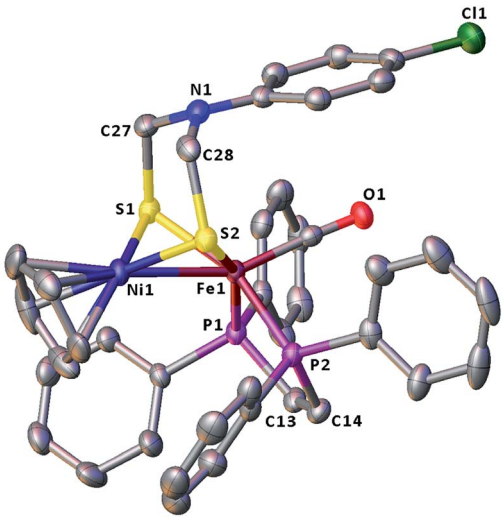

Fig. 3 Molecular structure of model complex **6** with ellipsoids drawn at a 50% probability level. All hydrogen atoms and the anion BF_4^- are omitted for clarity.

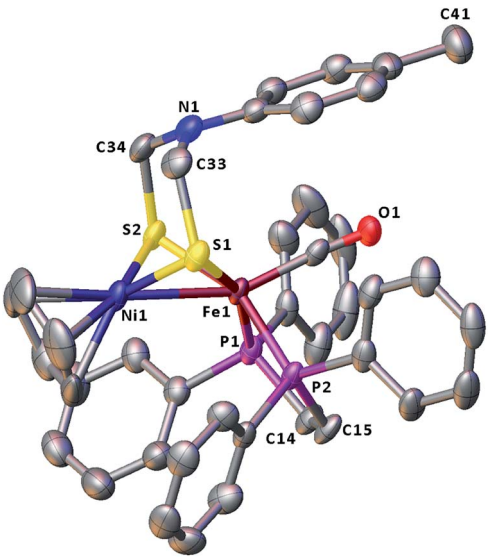

Fig. 4 Molecular structure of model complex **7** with ellipsoids drawn at a 50% probability level. All hydrogen atoms and the anion BF_4^- are omitted for clarity.

Open Access Article. Published on 28 August 2020. Downloaded on 5/25/2026 2:33:50 PM.
This article is licensed under a Creative Commons Attribution-NonCommercial 3.0 Unported Licence.

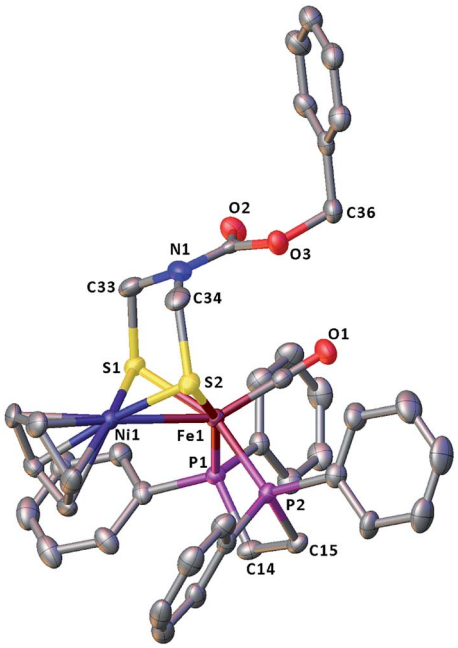

Fig. 5 Molecular structure of model complex **8** with ellipsoids drawn at a 50% probability level. All hydrogen atoms and the anion BF_4^- are omitted for clarity.

that (2.5145 Å) of the reported 1,3-propanedithiolato(pdt)-bridged analogue [CpNi(pdt)Fe(dppe)(CO)]BF_4.[40] Owing to the presence of a Ni–Fe metal–metal bond in **8**, the Ni center could be regarded as taking a "piano stool" geometry and the Fe center adopts a pseudo-octahedral geometry. In addition, the azadithiolato ligand in **8** is bridged between Ni and Fe atoms to construct two fused six-membered rings. The six-membered ring Fe1S1C33N1C34S2 shown in Fig. 3 possesses a boat conformation, whereas the six-membered ring Ni1S1C33N1C34S2 possesses a chair conformation. While the N-substituted CO_2CH_2Ph group is attached to the common N1 atom of the two fused six-membered rings with an axial type of bond, the terminal carbonyl ligand is bound to Fe1 atom in an axial position of the pseudo-octahedral geometry of the Fe center.

Electrochemical properties and electrocatalytic H_2 production catalyzed by model complexes 7 and 9

Although the electrochemical properties and electrocatalytic H_2 production for some [NiFe]-H_2ase models were previously studied by cyclic voltammetric techniques,[40–46] there isn't any studied result regarding the electrochemical and electrocatalytic properties of the azadithiolato-bridged [NiFe]-H_2ase models, so far. In order to see whether the prepared azadithiolato-bridged models **5–9** could have the electrocatalytic H_2-producing ability, we chose models **7** and **9** (note that they have the same type of structures as **5**, **6** and **8**) as representatives to study their electrochemical properties by CV techniques using the supporting electrolyte n-Bu_4NPF_6 in MeCN at a scan rate of 100 mVs^{-1}. As shown in Table 2 and Fig. 6, complex **7** displayed one quasi-reversible reduction wave at −1.07 V (due to its $|E_{pc} - E_{Pa}| = 82$ mV and $i_{pc}/i_{pa} = 1.05$),[47] one irreversible reduction wave at −1.98 V and one irreversible oxidation wave at 0.54 V, while complex **9** displayed one quasi-reversible reduction wave at −1.15 V (due to its $|E_{pc} - E_{Pa}| = 103$ mV and $i_{pc}/i_{pa} = 1.33$),[47] one irreversible reduction wave at −1.99 V, and one irreversible oxidation wave at 0.45 V, respectively. Previously, the electrochemical properties of the two pdt-bridged analogues of **7** and **9**, namely complexes [CpNi(pdt)Fe(dppv)(CO)]BF_4 (**A**) and [CpNi(pdt)Fe(dppe)(CO)]BF_4 (**B**) (see Table 2) were studied by cyclic voltammetry.[40] Similar to this case, the three redox events of **7** and **9** could be assigned to the $Ni^{II}Fe^{II}/Ni^{I}Fe^{II}$, $Ni^{I}Fe^{II}/Ni^{I}Fe^{I}$ and $Ni^{II}Fe^{II}/Ni^{III}/Fe^{II}$ couples, respectively.

Having determined the electrochemical properties of **7** and **9**, we further determined their cyclic voltammograms in the presence and absence (for comparison) of trifluoroacetic acid (TFA) ($pK_a^{MeCN} = 12.7$, $E^{\circ}_{HA} = -0.89$ V),[48,49] in order to see whether they could catalyze the proton reduction of TFA to give H_2. As shown in Fig. 7 and 8, when TFA was sequentially added from 2 to 10 mM to MeCN solutions of **7** and **9**, the current heights of their original first reduction waves were basically unchanged. However, in contrast to this, the current heights of their original second reduction waves were remarkably increased. Apparently, such an observation features an electrocatalytic proton reduction process from TFA to hydrogen.[41,43] Note that through comparison of the reduction potentials E_{pc} and peak currents i_p in the CVs of **7**/**9** with those in the CVs of TFA without **7**/**9** (see Fig. S1 and Table S1 in the ESI†), models **7**/

Table 2 Electrochemical data of **7**/**9**[a] and **A**/**B**[b]

Complex	E_{pc1}/V	E_{pc2}/V	E_{pa}/V
7	−1.07	−1.98	0.54
9	−1.15	−1.99	0.45
A[40]	−1.15	−2.18	0.72
B[40]	−1.16	−2.15	0.70

[a] All potentials are *versus* Fc/Fc^+ in 0.1 M n-Bu_4NPF_6/MeCN at a scan rate of 0.1 V s^{-1}. [b] All potentials are *versus* Fc/Fc^+ in 0.1 M n-Bu_4NPF_6/CH_2Cl_2 at a scan rate of 0.5 V s^{-1}.

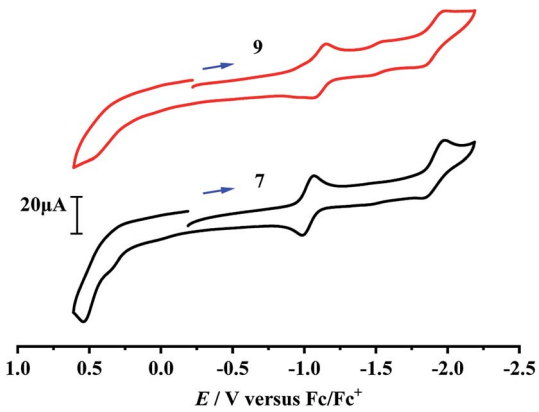

Fig. 6 Cyclic voltammograms of **7** and **9** (1.0 mM) in 0.1 M n-Bu_4NPF_6/MeCN at a scan rate of 0.1 V s^{-1}. Arrows indicate the starting potential and scan direction.

Open Access Article. Published on 28 August 2020. Downloaded on 5/25/2026 2:33:50 PM.
This article is licensed under a Creative Commons Attribution-NonCommercial 3.0 Unported Licence.

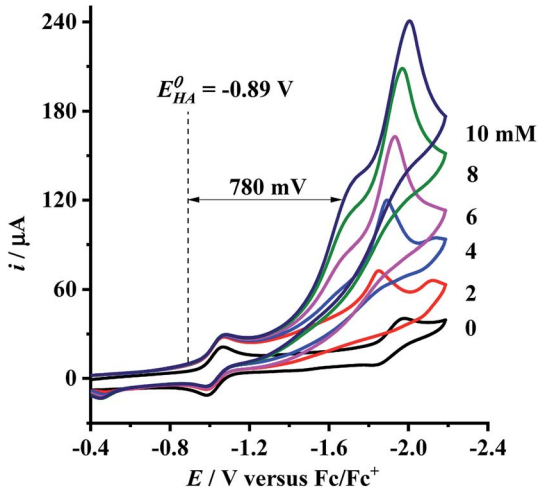

Fig. 7 Cyclic voltammograms of **7** (1.0 mM) with TFA (0–10 mM) in 0.1 M n-Bu_4NPF_6/MeCN at a scan rate of 0.1 V s^{-1}.

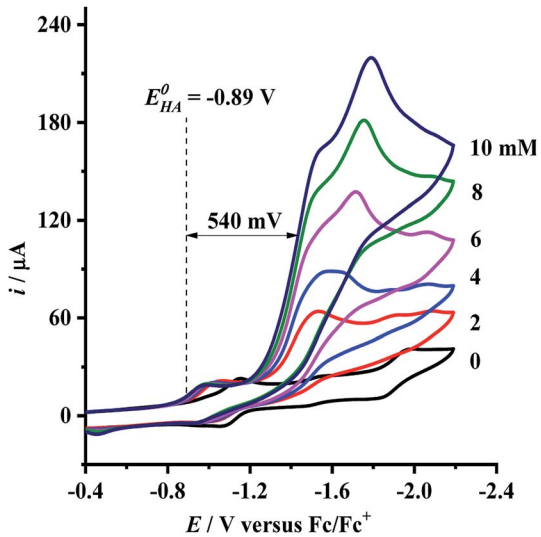

Fig. 8 Cyclic voltammograms of **9** (1.0 mM) with TFA (0–10 mM) in 0.1 M n-Bu_4NPF_6/MeCN at a scan rate of 0.1 V s^{-1}.

9 were further proved to be catalysts for proton reduction. In addition, during the proton reductions catalyzed by **7** and **9**, the original second reduction waves were positively shifted by *ca.* 15 and 45 mV, respectively; this is most likely due to protonation of the central N atoms in their bridged azadithiolato ligands.[50]

Recently, we[51] and others[52] reported that some mononuclear Fe complexes can serve as catalysts for proton reduction to hydrogen. In order to observe whether the mononuclear Fe precursors of model complexes **5–8** (namely complexes **1–4**) could catalyze the proton reductions, we chose complexes **3** and **4** as representatives to determine their cyclic voltammograms in the presence of TFA under the same conditions as those used for dertermination of models **7** and **9**. We found that when TFA was sequentially added from 2 to 10 mM to MeCN solutions of **3** and **4**, the current heights of the acid-induced reduction waves were considerably increased near their only one original reduction waves caused by their Fe(II)Fe(I) couples (see Fig. S2 and S3 in the ESI†). Obviously, such an observation demonstrates an electrocatalytic proton reduction process catalyzed by complexes **3** and **4**. So, we might conclude that for mononuclear Fe complexes **3** and **4**, only Fe makes contribution to their electrocatalytic proton reduction reactions caused by their Fe(II)/Fe(I) couples, while for dinuclear models **7** and **9**, both Ni and Fe make contribution to the electrocatalytic proton reduction reactions occurred near their original second reduction waves caused by their Ni(I)Fe(II)/Ni(I)Fe(I) couples.

To evaluate the electrocatalytic H_2-producing ability of **7** and **9**, we determined the ratio of the catalytic current (i_{cat}) to reductive peak current (i_p) in the absence of the added acid (note that a higher i_{cat}/i_p value indicates a faster catalysis).[53] At a concentration of 10 mM TFA, the i_{cat}/i_p values of **7** and **9** were calculated to be 6.0 and 5.3, respectively. It follows that the H_2-producing ability catalyzed by complex **7** (with a 4-MeC_6H_4N group and a dppv ligand) is higher than that catalyzed by **9** (with an NH group and a dppe ligand). However, in order to compare the electrocatalytic H_2-producing ability of the bridgehead N-substituted complex **8** with its parent complex **9**, we further determined its i_{cat}/i_p value by CV techniques to be 6.4 under the same conditions. Therefore, the H_2-producing ability of complex **8** with a stronger electron-attracting $PhCH_2CO_2N$ group is higher than that of complex **9** with a weaker electron-attracting NH group. In addition, at a 10 mM TFA concentration, the i_{cat}/i_p values (5.3–6.4) of complexes **7–9** are higher than those (*ca.* 4) of the previously reported analogues $[HNiFe(pdt)(dppe)(L)(CO)_2]BF_4$ (L = $P(OPh)_3$, PPh_3).[54]

Since overpotential is also an important parameter for evaluating the electrocatalytic ability for a catalyst (note that a better catalyst has a lower overpotential), we used Evans' method to calculate the overpotentials of **7** and **9** according to the following two equations:[49,55]

$$\text{Overpotential} = \left|E^{\circ}_{\text{cat}/2} - E^{\circ}_{\text{HA}}\right| \quad (1)$$

$$E^{\circ}_{\text{HA}} = E^{\circ}_{\text{H}^+/\text{H}_2} - \left(\frac{2.303RT}{F}\right)\text{p}K_{\text{a,HA}} \quad (2)$$

where $E_{cat/2}$ is the catalytic half-wave potential and E°_{HA} is the standard potential of the acid; R is the ideal gas constant 8.314 J mol^{-1} K^{-1}; T is the absolute temperature 298 K; F is the Faraday's constant 9.65×10^4 C mol^{-1}; in addition, the pK_a value of TFA in MeCN and the standard redox potential $E^{\circ}_{H^+/H_2}$ have been previously determined to be 12.7 (ref. 48) and −0.14 V,[49] respectively. According to eqn (2), the standard potential E°_{HA} can be calculated to be −0.89 V and then according to eqn (1), the overpotentials of **7** and **9** can be calculated to be 0.78 and 0.54 V, respectively (see Fig. 7 and 8). At a 10 mM acid concentration, overpotentials of our azadithiolato-bridged dinuclear NiFe complexes **7** (0.78 V) and **9** (0.54 V) by using TFA as proton source are higher than those (*ca.* 0.5 V) of the previously reported analogues $[HNiFe(pdt)(dppe)(L)(CO)_2]BF_4$ (L = $P(OPh)_3$, PPh_3) using TFA as proton source.[54] Particularly worth noting is that in terms of the studied results regarding the structure and catalytic function described above, complexes **7**

Open Access Article. Published on 28 August 2020. Downloaded on 5/25/2026 2:33:50 PM.
This article is licensed under a Creative Commons Attribution-NonCommercial 3.0 Unported Licence.

Table 3 Crystal data and structure refinement details for **6–8**

	6	**7**	**8**
Formula	$C_{40}H_{35}BClF_4FeNNiO$ P_2S_2	$C_{41}H_{38}BF_4FeNNiO$ $P_2S_2 \cdot CH_2Cl_2$	$C_{42}H_{40}BF_4FeNNiO_3$ $P_2S_2 \cdot CH_2Cl_2$
M_w	908.57	973.08	1019.10
Cryst syst	Monoclinic	Monoclinic	Triclinic
Space group	$P121/c1$	$P121/c1$	$P\bar{1}$
a (Å)	17.861(4)	17.8793(11)	10.113(2)
b (Å)	11.063(2)	11.0429(5)	12.365(3)
c (Å)	22.252(5)	22.4895(10)	18.383(4)
α (°)	90	90	75.55(3)
β (°)	108.15(3)	108.615(6)	87.96(3)
γ (°)	90	90	77.76(3)
V (Å^3)	4178.2(16)	4208.0(4)	2175.1(8)
Z	4	4	2
Crystal size (mm)	0.05 × 0.04 × 0.03	0.06 × 0.05 × 0.03	0.20 × 0.18 × 0.12
D_c (g cm^{-3})	1.444	1.536	1.556
μ (mm^{-1})	1.088	1.148	1.117
F(000)	1856	1992	1044
Reflns collected	49 278	43 090	26 271
Reflns unique	9958	8586	10 291
$\theta_{min/max}$ (°)	2.078/27.863	1.905/26.372	1.144/27.834
Final R	0.0693	0.0712	0.0567
Final R_W	0.1648	0.1987	0.1575
GOF on F^2	1.127	1.061	1.060
$\Delta\rho_{max/min}$ (e Å^{-3})	0.536/−0.576	1.000/−1.039	0.738/−1.255

and **9** might be regarded as not only the structural models but also the functional models for the active site of [NiFe]-H_2ases.

Summary and conclusion

We have synthesized the first azadithiolato-bridged dinuclear NiFe model complexes **5–8** and **9** by reactions of the N-substituted azadithiolato-chelated mononuclear Fe complexes **1–4** with $Cp_2Ni/HBF_4 \cdot Et_2O$ and by reaction of the N-substituted azadithiolato-bridged complex **8** with $HBF_4 \cdot Et_2O$, respectively. Particularly worth noting is that the spectroscopic characterization of all the new model complexes **5–9** and the X-ray crystallographic study on their three representative complexes **6–8** have proved that models **5–9** indeed contain an azadithiolato ligand that is bridged between their NiFe centers to form a butterfly Ni(II)S_2Fe(II) cluster core with a Ni–Fe metal–metal bond. In addition, from the electrochemical and electrocatalytic studies, the two representative models **7** and **9** have been found to be catalysts for proton reduction to hydrogen using TFA as the proton source under electrochemical conditions. Therefore, according to the structural and functional similarity with the active site of [NiFe]-H_2ases, complexes **5–9** might be regarded as the structural and functional models of [NiFe]-H_2ases.

Experimental section

General comments

All reactions were carried out using standard Schlenk and vacuum-line techniques under an atmosphere of argon. While tetrahydrofuran (THF) and Et_2O were distilled under Ar from sodium/benzophenone ketyl, CH_2Cl_2 was distilled from CaH_2. *t*-BuONa, $(\eta5\text{-}C_5H_5)_2Ni$, $HBF_4 \cdot Et_2O$ (50–55% w/w in Et_2O), anhydrous $FeCl_2$ and other chemicals were commercially available and used as received. $RN[CH_2S(O)CMe]_2$ (R = Ph,[56] 4-ClC_6H_4,[57] CO_2CH_2Ph,[58] (dppv)$Fe(CO)_2Cl_2$ (dppv = 1,2-bis(diphenylphosphino)ethene)[35] and (dppe)$Fe(CO)_2Cl_2$ (dppe = 1,2-bis(diphenylphosphino)ethane)[36]) were prepared according to the published procedures. While ^1H, $^{13}C\{^1H\}$, and $^{31}P\{^1H\}$ NMR spectra were obtained on a Bruker Avance 400 NMR spectrometer, IR spectra were recorded on a Bio-Rad FTS 135 infrared spectrophotometer. Elemental analyses were performed on an Elementar Vario EL analyzer. Melting points were determined on a SGW X-4 microscopic melting point apparatus and were uncorrected.

Preparation of $[PhN(CH_2S)_2]Fe(CO)_2$(dppv) (1). A 250 mL Schlenk flask was charged with $FeCl_2$ (0.634 g, 5.0 mmol) in 100 mL acetone and dppv (1.98 g, 5.0 mmol) in 20 mL of THF. The mixture was stirred at room temperature and bubbled with CO gas for 4 h to give a (dppv)$Fe(CO)_2Cl_2$-containing brown-red solution. Additionally, a 100 mL Schlenk flask was charged with thioester $PhN[CH_2S(O)CMe]_2$ (2.02 g, 7.5 mmol), sodium *tert*-butoxide (1.44 g, 15.0 mmol), and 40 mL of THF. The mixture was stirred at −78 °C for 4 h to give a $PhN(CH_2SNa)_2$-containing pale yellow solution. To the *in situ* prepared (dppv)$Fe(CO)_2Cl_2$-containing solution cooled to −78 °C was slowly added the prepared $PhN(CH_2SNa)_2$-containing solution and then the mixture was stirred at −78 °C for 5 h. Solvent was removed at reduced pressure and the residue was subjected to column chromatography (silica gel). Elution with CH_2Cl_2 developed a red band, from which **1** (0.622 g, 18%) was obtained as a brown-red solid, mp 93–94 °C. Anal. calcd for $C_{36}H_{31}FeNO_2P_2S_2$: C, 62.52; H, 4.52; N, 2.03. Found: C, 62.35; H, 4.65; N, 2.00. IR (KBr disk): $\nu_{C\equiv O}$ 2018 (w), 1973 (*vs.*) cm^{-1}. ^1H NMR (400

Open Access Article. Published on 28 August 2020. Downloaded on 5/25/2026 2:33:50 PM. This article is licensed under a Creative Commons Attribution-NonCommercial 3.0 Unported Licence.

MHz, $CDCl_3$): 4.63 (s, 4H, CH_2NCH_2), 6.69–7.91 (m, 27H, CH=CH, $5C_6H_5$) ppm. $^{13}C\{^1H\}$ NMR (100 MHz, $CDCl_3$): 48.6 (s, CH_2NCH_2), 114.7–134.7 (m, C_6H_5), 146.3–150.8 (m, CH=CH), 211.8, 212.2 (2s, C≡O) ppm. $^{31}P\{^1H\}$ NMR (162 MHz, $CDCl_3$): 79.9 (s, FeP) ppm.

Preparation of [4-$ClC_6H_4N(CH_2S)_2$]$Fe(CO)_2$(dppv) (2). The same procedure was followed as for the preparation of **1**, except that 4-$ClC_6H_4N[CH_2S(O)CMe]_2$ (2.28 g, 7.5 mmol) was used instead of $PhN[CH_2S(O)CMe]_2$. **2** (0.835 g, 23%) was obtained as a brown-red solid, mp 145–146 °C. Anal. calcd for $C_{36}H_{30}ClFeNO_2P_2S_2$: C, 59.56; H, 4.17; N, 1.93. Found: C, 59.47; H, 4.21; N, 1.69. IR (KBr disk): $\nu_{C\equiv O}$ 2020 (w), 1973 (*vs.*) cm^{-1}. ^1H NMR (400 MHz, $CDCl_3$): 4.57 (s, 4H, CH_2NCH_2), 6.61–7.78 (m, 26H, CH=CH, $4C_6H_5$, C_6H_4) ppm. $^{13}C\{^1H\}$ NMR (100 MHz, DMSO-d_6): 48.0 (s, CH_2NCH_2), 115.5–144.1 (m, C_6H_5, C_6H_4), 150.2–150.6 (m, CH=CH), 212.2 (s, C≡O) ppm. $^{31}P\{^1H\}$ NMR (162 MHz, $CDCl_3$): 80.0 (s, FeP) ppm.

Preparation of [4-$MeC_6H_4N(CH_2S)_2$]$Fe(CO)_2$(dppv) (3). In order to prepare **3**, we should first prepare its precursor, the new bis(thioester) 4-$MeC_6H_4N[CH_2S(O)CMe]_2$. (i) Preparation of 4-$MeC_6H_4N[CH_2S(O)CMe]_2$: a 250 mL three-necked flask was charged with 4-$MeC_6H_4NH_2$ (10.7 g, 100 mmol), 37% aqueous formaldehyde (24.2 mL, 320 mmol), thioacetic acid (14.6 mL, 200 mmol), and ethanol (100 mL). While stirring, the mixture was heated to about 60 °C and stirred at this temperature for 3 h. To the resulting mixture was added 100 mL of ice-water to give some precipitates. The precipitates were collected by filtration, washed with some cold ethanol, and finally dried under vacuum to give 4-$MeC_6H_4N[CH_2S(O)CMe]_2$ (25.6 g, 90%) as a white solid, mp 66–67 °C. Anal. calcd for $C_{13}H_{17}NO_2S_2$: C, 55.10; H, 6.05; N, 4.95. Found: C, 55.35; H, 6.30; N, 4.66. IR (KBr disk): $\nu_{C=O}$ 1688 (*vs.*) cm^{-1}. ^1H NMR (400 MHz, $CDCl_3$): 2.27 (s, 3H, $CH_3C_6H_4$), 2.36 (s, 6H, $2CH_3C{=}O$), 5.10 (s, 4H, CH_2NCH_2), 6.68–7.10 (m, 4H, C_6H_4) ppm. $^{13}C\{^1H\}$ NMR (100 MHz, $CDCl_3$): 20.5 (s, $CH_3C_6H_4$), 31.4 (s, $CH_3C{=}O$), 53.1 (s, CH_2NCH_2), 114.7–141.6 (m, C_6H_4), 196.1 (s, C=O) ppm. (ii) Preparation of **3**: the same procedure was followed as for the preparation of **1**, except that 4-$MeC_6H_4N[CH_2S(O)CMe]_2$ (2.13 g, 7.5 mmol) was employed in place of $PhN[CH_2S(O)CMe]_2$. **3** (0.741 g, 21%) was obtained as a brown-red solid, mp 113–114 °C. Anal. calcd for $C_{37}H_{33}FeNO_2P_2S_2$: C, 62.98; H, 4.71; N, 1.99. Found: C, 62.72; H, 4.95; N, 2.05. IR (KBr disk): $\nu_{C\equiv O}$ 2035 (w), 1973 (*vs.*) cm^{-1}. ^1H NMR (400 MHz, acetone-d_6): 2.18 (s, 3H, CH_3), 4.56 (s, 4H, CH_2NCH_2), 6.92–7.80 (m, 24H, $4C_6H_5$, C_6H_4), 8.17–8.31 (m, 2H, CH=CH) ppm. $^{13}C\{^1H\}$ NMR (100 MHz, DMSO-d_6): 17.7 (s, CH_3), 45.9 (s, CH_2NCH_2), 113.1–131.6 (m, C_6H_5, C_6H_4), 144.7–145.8 (m, CH=CH), 200.1 (s, C≡O) ppm. $^{31}P\{^1H\}$ NMR (162 MHz, $CDCl_3$): 77.9 (s, FeP) ppm.

Preparation of [$PhCH_2O_2CN(CH_2S)_2$]$Fe(CO)_2$(dppe) (4). The same procedure was followed as for the preparation of **1**, except that $PhCH_2O_2CN[CH_2S(O)CMe]_2$ (2.46 g, 7.5 mmol) was used in place of $PhN[CH_2S(O)CMe]_2$. **4** (1.32 g, 35%) was obtained as a brown-red solid, mp 91–92 °C. Anal. calcd for $C_{38}H_{35}FeNO_4P_2S_2$: C, 60.73; H, 4.69; N, 1.86. Found: C, 60.42; H, 4.94; N, 1.66. IR (KBr disk): $\nu_{C\equiv O}$ 2013 (*vs.*), 1968 (*vs.*); $\nu_{C=O}$ 1700 (*vs.*) cm^{-1}. ^1H NMR (400 MHz, $CDCl_3$): 3.02–4.56 (m, 6H, PCH_2CH_2P, OCH_2); 4.89–5.30 (m, 4H, CH_2NCH_2); 7.30–7.76 (m, 25H, $5C_6H_5$) ppm. $^{13}C\{^1H\}$ NMR (100 MHz, $CDCl_3$): 24.6–57.0 (m, PCH_2CH_2P, OCH_2), 66.7–68.0 (m, CH_2NCH_2), 127.2–154.7 (m, C_6H_5), 210.8 (s, C=O), 213.0, 213.3 (2s, C≡O) ppm. $^{31}P\{^1H\}$ NMR (162 MHz, $CDCl_3$): 44.3 (s, FeP) ppm.

Preparation of [CpNi{(μ-$SCH_2)_2NPh$}Fe(CO)(dppv)]BF_4 (5). While stirring, nickelocene (0.038 g, 0.2 mmol) was dissolved in diethyl ether (5 mL) and then $HBF_4 \cdot Et_2O$ (27.2 μL, 0.2 mmol) was added. After the mixture was stirred at room temperature for 15 min, a brown-red suspension was formed. To this suspension was added a solution of **1** (0.138 g, 0.2 mmol) in CH_2Cl_2 (5 mL). The new mixture was stirred at room temperature for 2 h, solvent was removed at reduced pressure to give a residue, which was subjected to column chromatography (silica gel), elution with CH_2Cl_2/acetone (v/v = 10 : 1) developed a major red band, from which **5** (0.052 g, 30%) was obtained as brown-red solid. Mp 220–221 °C. Anal. calcd for $C_{40}H_{36}BF_4FeNNiOP_2S_2$: C, 54.96; H, 4.15; N, 1.60. Found: C, 54.86; H, 3.98; N, 1.62. IR (KBr disk): $\nu_{C\equiv O}$ 1956 (m) cm^{-1}. ^1H NMR (400 MHz, acetone-d_6): 4.43 (s, 5H, C_5H_5), 4.68, 5.47 (dd, J = 14.6 Hz, 4H, CH_2NCH_2), 6.77–8.13 (m, 25H, $5C_6H_5$), 8.71, 8.86 (2s, 2H, CH=CH) ppm. $^{13}C\{^1H\}$ NMR (100 MHz, DMSO-d_6): 54.4 (s, CH_2NCH_2), 94.5, 95.9 (2s, C_5H_5), 115.4–142.2 (m, C_6H_5), 149.3–149.9 (m, CH=CH), 205.9 (s, C≡O) ppm. $^{31}P\{^1H\}$ NMR (162 MHz, $CDCl_3$): 82.7 (s, FeP) ppm.

Preparation of [CpNi{(μ-$SCH_2)_2NC_6H_4Cl$-4}Fe(CO)(dppv)]BF_4 (6). The same procedure was followed as for the preparation of **5**, except that **2** (0.145 g, 0.2 mmol) was utilized instead of **1**. Complex **6** (0.113 g 62%) was obtained as a brown-red solid, mp 197–198 °C. Anal. calcd for $C_{40}H_{35}BClF_4FeNNiOP_2S_2$: C, 52.88; H, 3.88; N, 1.54. Found: C, 52.84; H, 4.01; N, 1.62. IR (KBr disk): $\nu_{C\equiv O}$ 1952 (m) cm^{-1}. ^1H NMR (400 MHz, acetone-d_6): 4.47 (s, 5H, C_5H_5), 4.64, 5.49 (dd, 4H, J = 15.4 Hz, CH_2NCH_2), 7.32–8.13 (m, 24H, $4C_6H_5$, C_6H_4), 8.73, 8.88 (2s, 2H, CH=CH) ppm. $^{13}C\{^1H\}$ NMR (100 MHz, CD_2Cl_2): 52.6, 54.1 (2s, CH_2NCH_2), 94.8, 96.5 (2s, C_5H_5), 117.0–142.4 (m, C_6H_5, C_6H_4), 149.4–151.3 (m, CH=CH), 210.9 (s, C≡O) ppm. $^{31}P\{^1H\}$ NMR (162 MHz, $CDCl_3$): 83.9 (s, FeP) ppm.

Preparation of [CpNi{(μ-$SCH_2)_2NC_6H_4Me$-4}Fe(CO)(dppv)]BF_4 (7). The same procedure was followed as for the preparation of **5**, except that **3** (0.141 g, 0.2 mmol) was employed in place of **1**. Complex **7** (0.038 g, 21%) was obtained as a brown-red solid, mp 210–211 °C. Anal. calcd for $C_{41}H_{38}BF_4FeNNiOP_2S_2$: C, 55.45; H, 4.31; N, 1.58. Found: C, 55.23; H, 4.28; N, 1.34. IR (KBr disk): $\nu_{C\equiv O}$ 1955 (s) cm^{-1}. ^1H NMR (400 MHz, acetone-d_6): 2.12 (s, 3H, CH_3), 4.42 (s, 5H, C_5H_5), 4.67, 5.41 (dd, 4H, J = 13.0 Hz, CH_2NCH_2), 7.14–8.13 (m, 24H, $4C_6H_5$, C_6H_4), 8.69–8.84 (m, 2H, CH=CH) ppm. $^{13}C\{^1H\}$ NMR (100 MHz, CD_3CN): 20.1 (s, CH_3), 54.8 (s, CH_2NCH_2), 96.1 (s, C_5H_5), 117.0–141.5 (m, C_6H_5, C_6H_4), 150.5–151.2 (m, CH=CH), 219.5 (s, C≡O) ppm. $^{31}P\{^1H\}$ NMR (162 MHz, $CDCl_3$): 83.7 (s, FeP) ppm.

Preparation of [CpNi{(μ-$SCH_2)_2NCO_2CH_2Ph$}Fe(CO)(dppe)]BF_4 (8). The same procedure was followed as for the preparation of **5**, except that **4** (0.150 g, 0.2 mmol) was used instead of **1**. Complex **8** (0.052 g, 28%) was obtained as a brown-red solid, mp 121–122 °C. Anal. calcd for $C_{42}H_{40}BF_4FeNNiO_3P_2S_2$: C, 54.00; H, 4.32; N, 1.50. Found: C, 54.27; H, 4.43; N, 1.58. IR (KBr disk): $\nu_{C\equiv O}$ 1940 (*vs.*); $\nu_{C=O}$ 1704 (*vs.*) cm^{-1}. ^1H NMR (400 MHz,

Open Access Article. Published on 28 August 2020. Downloaded on 5/25/2026 2:33:50 PM. This article is licensed under a Creative Commons Attribution-NonCommercial 3.0 Unported Licence.

$CDCl_3$): 3.03–4.05 (m, 6H, PCH_2CH_2P, OCH_2), 4.54 (s, 5H, C_5H_5), 4.98–5.31 (m, 4H, CH_2NCH_2), 7.12–7.86 (m, 25H, $5C_6H_5$) ppm. $^{13}C\{^1H\}$ NMR (100 MHz, CD_3CN): 29.5, 29.8 (2s, PCH_2CH_2P), 50.7 (s, CH_2NCH_2), 69.5 (s, OCH_2), 96.5 (s, C_5H_5), 128.9–154.1 (m, C_6H_5), 211.0 (s, C═O), 216.4 (s, C≡O) ppm. $^{31}P\{^1H\}$ NMR (162 MHz, $CDCl_3$): 78.3, 79.1 (2s, FeP) ppm.

Preparation of [CpNi{(μ-SCH_2)$_2$NH}Fe(CO)(dppe)]BF_4 (9). To a solution of **8** (0.093 g, 0.1 mmol) in CH_2Cl_2 (5 mL) were added PhOMe (0.5 mL) and $HBF_4 \cdot Et_2O$ (408 μL, 3.0 mmol). The mixture was stirred at room temperature for 4 h to give a brown-red solution. Solvents were removed to give a residue, which was subjected to column chromatography (silica gel). Elution with CH_2Cl_2/acetone developed a major red band, from which **9** (0.034 g, 42%) was obtained as a brown-red solid, mp 170 °C (dec). Anal. calcd for $C_{34}H_{34}BF_4FeNNiOP_2S_2$: C, 51.04; H, 4.28; N, 1.75. Found: C, 50.81; H, 4.56; N, 1.70. IR (KBr disk): $\nu_{C\equiv O}$ 1939 (*vs.*) cm^{-1}. ^1H NMR (400 MHz, CD_3CN): 2.26 (br.s, 1H, NH), 3.04–4.42 (m, 8H, PCH_2CH_2P, CH_2NCH_2), 4.61 (s, 5H, C_5H_5), 7.43–7.95 (m, 20H, $4C_6H_5$) ppm. $^{13}C\{^1H\}$ NMR (100 MHz, CD_3CN): 29.2, 29.6 (2s, PCH_2CH_2P), 52.4 (s, CH_2NCH_2), 95.7 (s, C_5H_5), 129.2–133.8 (m, C_6H_5), 218.3 (s, C≡O) ppm. $^{31}P\{^1H\}$ NMR (162 MHz, acetone-d_6): 78.1 (s, FeP) ppm.

Electrochemical and electrocatalytic experiments

Acetonitrile (Amethyst Chemicals, HPLC grade) for electrochemical and electrocatalytic experiments was used directly without further purification. A solution of 0.1 M *n*-Bu_4NPF_6 in MeCN was used as the electrolyte in all CV experiments. The *n*-Bu_4NPF_6 electrolyte was dried in an oven at 110 °C for at least 24 h. Dry N_2 was purged through the solutions for at least 10 min before the measurements were taken. The measurements were made by using a BAS Epsilon potentiostat. All voltammograms were obtained in a three-electrode cell with a 3 mm diameter glass carbon working electrode, a platinum counter electrode, and a Ag/Ag^+ (0.01 M $AgNO_3$/0.1 M *n*-Bu_4NPF_6 in MeCN) reference electrode under an atmosphere of nitrogen. The working electrode was polished with 0.05 μm alumina paste and sonicated in water for about 10 min prior to use. All potentials are quoted against Fc/Fc^+ potential.

X-ray crystal structure determinations of 6–8

While single crystals of **6–8** for X-ray diffraction analysis were grown by slow diffusion of hexane into their CH_2Cl_2 solutions at −5 °C. A single crystal of **6–8** was mounted on a Rigaku MM-007 (rotating anode) diffractometer equipped with a Bruker P4 accessory. While the data of **6** and **8** were collected using a confocal monochromator with Mo Kα radiation (λ = 0.71073 Å) in the ω scanning mode at 113 K, data of **7** were collected using a confocal monochromator with Mo Kα radiation (λ = 0.71073 Å) in the ω scanning mode at 293 K, respectively. Data collection, reduction, and absorption correction were performed by the CRYSTALCLEAR program.[59] The structures were solved by direct methods using the SHELXS program[60] and refined by full-matrix least-squares techniques (SHELXL)[61] on F^2. Hydrogen atoms were located by using the geometric method. Details of crystal data, data collections, and structure refinements are summarized in Table 3.

Conflicts of interest

There are no conflicts of interest to declare.

Acknowledgements

We are grateful to the National Natural Science Foundation of China (21772106) and the Ministry of Science and Technology of China (973 program 2014CB845604) for financial support.

References

1 R. Cammack, *Nature*, 1999, **397**, 214–215.
2 J. C. Fontecilla-Camps, A. Volbeda, C. Cavazza and Y. Nicolet, *Chem. Rev.*, 2007, **107**, 4273–4303.
3 W. Lubitz, H. Ogata, O. Rüdiger and E. Reijerse, *Chem. Rev.*, 2014, **114**, 4081–4148.
4 A. Volbeda, M.-H. Charon, C. Piras, E. C. Hatchikian, M. Frey and J. C. Fontecilla-Camps, *Nature*, 1995, **373**, 580–587.
5 A. Volbeda, E. Garcin, C. Piras, A. L. de Lacey, V. M. Fernandez, E. C. Hatchikian, M. Frey and J. C. Fontecilla-Camps, *J. Am. Chem. Soc.*, 1996, **118**, 12989–12996.
6 A. Volbeda, L. Martin, C. Cavazza, M. Matho, B. W. Faber, W. Roseboom, S. P. J. Albracht, E. Garcin, M. Rousset and J. C. Fontecilla-Camps, *J. Biol. Inorg Chem.*, 2005, **10**, 239–249.
7 R. Cammack, M. Frey and R. Robson, *Hydrogen as a fuel: Learning from nature*, Taylor & Francis, London, 2001.
8 J. A. Turner, *Science*, 2004, **305**, 972–974.
9 W. Lubitz and W. Tumas, *Chem. Rev.*, 2007, **107**, 3900–3903.
10 T. R. Simmons, G. Berggren, M. Bacchi, M. Fontecave and V. Artero, *Coord. Chem. Rev.*, 2014, **270–271**, 127–150.
11 S. Ogo, *Coord. Chem. Rev.*, 2017, **334**, 43–53.
12 D. Schilter, J. M. Camara, M. T. Huynh, S. Hammes-Schiffer and T. B. Rauchfuss, *Chem. Rev.*, 2016, **116**, 8693–8749.
13 N. J. Lindenmaier, S. Wahlefeld, E. Bill, T. Szilvási, C. Eberle, S. Yao, P. Hildebrandt, M. Horch, I. Zebger and M. Driess, *Angew. Chem., Int. Ed.*, 2017, **56**, 2208–2211.
14 C. U. Perotto, G. Marshall, G. J. Jones, E. S. Davies, W. Lewis, J. McMaster and M. Schröder, *Chem. Commun.*, 2015, **51**, 16988–16991.
15 C. U. Perotto, C. L. Sodipo, G. J. Jones, J. P. Tidey, A. J. Blake, W. Lewis, E. S. Davies, J. McMaster and M. Schröder, *Inorg. Chem.*, 2018, **57**, 2558–2569.
16 F. Osterloh, W. Saak, D. Haase and S. Pohl, *Chem. Commun.*, 1997, 979–980.
17 L.-C. Song, Y. Lu, L. Zhu and Q.-L. Li, *Organometallics*, 2017, **36**, 750–760.
18 J. Jiang, M. Maruani, J. Solaimanzadeh, W. Lo, S. A. Koch and M. Millar, *Inorg. Chem.*, 2009, **48**, 6359–6361.
19 D. Sellmann, F. Geipel, F. Lauderbach and F. W. Heinemann, *Angew. Chem., Int. Ed.*, 2002, **41**, 632–634.

Open Access Article. Published on 28 August 2020. Downloaded on 5/25/2026 2:33:50 PM.
This article is licensed under a Creative Commons Attribution-NonCommercial 3.0 Unported Licence.

20 L.-C. Song, X.-Y. Gao, W.-B. Liu, H.-T. Zhang and M. Cao, *Organometallics*, 2018, **37**, 1050–1061.
21 M. C. Smith, J. E. Barclay, S. P. Cramer, S. C. Davies, W.-W. Gu, D. L. Hughes, S. Longhurst and D. J. Evans, *J. Chem. Soc., Dalton Trans.*, 2002, 2641–2647.
22 J. A. W. Verhagen, M. Lutz, A. L. Spek and E. Bouwman, *Eur. J. Inorg. Chem.*, 2003, 3968–3974.
23 Z. Li, Y. Ohki and K. Tatsumi, *J. Am. Chem. Soc.*, 2005, **127**, 8950–8951.
24 D. Sellmann, F. Lauderbach and F. W. Heinemann, *Eur. J. Inorg. Chem.*, 2005, 371–377.
25 S. Ogo, K. Ichikawa, T. Kishima, T. Matsumoto, H. Nakai, K. Kusaka and T. Ohhara, *Science*, 2013, **339**, 682–684.
26 Y. Ohki, K. Yasumura, M. Ando, S. Shimokata and K. Tatsumi, *Proc. Natl. Acad. Sci. U. S. A.*, 2010, **107**, 3994–3997.
27 D. Brazzolotto, L. Wang, H. Tang, M. Gennari, N. Queyriaux, C. Philouze, S. Demeshko, F. Meyer, M. Orio, V. Artero, M. B. Hall and C. Duboc, *ACS Catal.*, 2018, **8**, 10658–10667.
28 D. Brazzolotto, M. Gennari, N. Queyriaux, T. R. Simmons, J. Pécaut, S. Demeshko, F. Meyer, M. Orio, V. Artero and C. Duboc, *Nat. Chem.*, 2016, **8**, 1054–1060.
29 (*a*) L.-C. Song, X.-Y. Yang, M. Cao, X.-Y. Gao, B.-B. Liu, L. Zhu and F. Jiang, *Chem. Commun.*, 2017, **53**, 3818–3821; (*b*) L.-C. Song, X.-Y. Yang, X.-Y. Gao and M. Cao, *Inorg. Chem.*, 2019, **58**, 39–42; (*c*) L.-C. Song, X.-J. Sun, P.-H. Zhao, J.-P. Li and H.-B. Song, *Dalton Trans.*, 2012, **41**, 8941–8950.
30 H.-J. Fan and M. B. Hall, *J. Am. Chem. Soc.*, 2001, **123**, 3828–3829.
31 A. Silakov, B. Wenk, E. Reijerse and W. Lubitz, *Phys. Chem. Chem. Phys.*, 2009, **11**, 6592–6599.
32 G. Berggren, A. Adamska, C. Lambertz, T. R. Simmons, J. Esselborn, M. Atta, S. Gambarelli, J.-M. Mouesca, E. Reijerse, W. Lubitz, T. Happe, V. Artero and M. Fontecave, *Nature*, 2013, **499**, 66–69.
33 L. P. Battaglia, G. P. Chiusoli, D. Delledonne, M. Nardelli, C. Pelizzi and G. Predieri, *Gazz. Chim. Ital.*, 1989, **119**, 345–348.
34 T. A. Manuel, *Inorg. Chem.*, 1963, **2**, 854–858.
35 A. Salzer and H. Werner, *Angew. Chem., Int. Ed.*, 1972, **11**, 930–932.
36 C. Elschenbroich, *Organometallics. Third, Completely Revised and Extended Edition*, WILEY-VCH Verlag GMBH & Co. KGdt, Weinheim Germany, 2006, p. 506.
37 C. Fichtner, C. Laurich, E. Bothe and W. Lubitz, *Biochemistry*, 2006, **45**, 9706–9716.
38 H. Ogata, K. Nishikawa and W. Lubitz, *Nature*, 2015, **520**, 571–574.
39 B. Cordero, V. Gómez, A. E. Platero-Prats, M. Revés, J. Echeverría, E. Cremades, F. Barragán and S. Alvarez, *Dalton Trans.*, 2008, 2832–2838.
40 G. M. Chambers, M. T. Huynh, Y. Li, S. Hammes-Schiffer, T. B. Rauchfuss, E. Reijerse and W. Lubitz, *Inorg. Chem.*, 2016, **55**, 419–431.
41 L.-C. Song, X.-F. Han, W. Chen, J.-P. Li and X.-Y. Wang, *Dalton Trans.*, 2017, **46**, 10003–10013.
42 M. E. Carroll, B. E. Barton, D. L. Gray, A. E. Mack and T. B. Rauchfuss, *Inorg. Chem.*, 2011, **50**, 9554–9563.
43 L.-C. Song, M. Cao and Y.-X. Wang, *Dalton Trans.*, 2015, **44**, 6797–6808.
44 S. Canaguier, L. Vaccaro, V. Artero, R. Ostermann, J. Pécaut, M. J. Field and M. Fontecave, *Chem.-Eur. J.*, 2009, **15**, 9350–9364.
45 M. Y. Darensbourg, I. Font, D. K. Mills, M. Pala and J. H. Reibenspies, *Inorg. Chem.*, 1992, **31**, 4965–4971.
46 B. Adhikary, S. Liu and C. R. Lucas, *Inorg. Chem.*, 1993, **32**, 5957–5962.
47 P. Zanello, *Inorganic Electrochemistry. Theory, Practice and Application*, Thomas Graham House, Cambridge, UK, 2003.
48 K. Izutsu, *Acid-Base Dissociation Constants in Dipolar Aprotic Solvents*, Blackwell Scientific Publications, Oxford, UK, 1990.
49 G. A. N. Felton, R. S. Glass, D. L. Lichtenberger and D. H. Evans, *Inorg. Chem.*, 2006, **45**, 9181–9184.
50 W. Dong, M. Wang, T. Liu, X. Liu, K. Jin and L. Sun, *J. Inorg. Biochem.*, 2007, **101**, 506–513.
51 (*a*) L.-C. Song, L. Zhu, F.-Q. Hu and Y.-X. Wang, *Inorg. Chem.*, 2017, **56**, 15216–15230; (*b*) L.-C. Song, F.-Q. Hu, M.-M. Wang, Z.-J. Xie, K.-K. Xu and H.-B. Song, *Dalton Trans.*, 2014, **43**, 8062–8071.
52 (*a*) S. C. Eady, T. Breault, L. Thompson and N. Lehnert, *Dalton Trans.*, 2016, **45**, 1138–1151; (*b*) S. Kaur-Ghumaan, L. Schwartz, R. Lomoth, M. Stein and S. Ott, *Angew. Chem., Int. Ed.*, 2010, **49**, 8033–8036.
53 G. A. N. Felton, C. A. Mebi, B. J. Petro, A. K. Vannucci, D. H. Evans, R. S. Glass and D. L. Lichtenberger, *J. Organomet. Chem.*, 2009, **694**, 2681–2699.
54 B. E. Barton and T. B. Rauchfuss, *J. Am. Chem. Soc.*, 2010, **132**, 14877–14885.
55 E. S. Rountree, B. D. McCarthy, T. T. Eisenhart and J. L. Dempsey, *Inorg. Chem.*, 2014, **53**, 9983–10002.
56 L.-C. Song, W.-B. Liu and B.-B. Liu, *Organometallics*, 2020, **39**, 1431–1439.
57 T. Izawa, Y. Terao and K. Suzuki, *Tetrahedron: Asymmetry*, 1997, **8**, 2645–2648.
58 C. Sommer, C. P. Richers, W. Lubitz, T. B. Rauchfuss and E. J. Reijerse, *Angew. Chem., Int. Ed.*, 2018, **57**, 5429–5432.
59 Rigaku Americas and Rigaku, *CrystalClear and CrystalStructure*, Rigaku and Rigaku Americas, The Woodlands, TX, 2007.
60 (*a*) G. M. Sheldrick, *SHELXS97, Program for Crystal Structure Solution,* University of Göttingen, Germany, 1997; (*b*) G. M. Sheldrick, *Acta Crystallogr., Sect. A: Found. Crystallogr.*, 2008, **64**, 112–122.
61 G. M. Sheldrick, *Acta Crystallogr., Sect. A: Found. Adv.*, 2015, **71**, 3–8.